Supplementary Information

Phase-Transition-Induced Dynamic Surface Wrinkle Pattern on Gradient Photo-Crosslinking Liquid Crystal Elastomer

Tao Wen,[1,2] Tianjiao Ma,[2,*] Jie Qian,[2], Zhaoxin Song,[3] Xuesong Jiang,[2,*] Yuan Yao[1,*]

[1]School of Materials Science and Engineering, East China University of Science and Technology, Shanghai 200237, China

E-mail: yaoyuan@ecust.edu.cn

[2]School of Chemistry & Chemical Engineering, Frontiers Science Center for Transformative Molecules, State Key Laboratory for Metal Matrix Composite Materials, Shanghai Jiao Tong University, Shanghai 200240, China

E-mail: skn-08284869@sjtu.edu.cn

E-mail: ponygle@sjtu.edu.cn

[3]State Key Laboratory of Separation Membranes and Membrane Processes, School of Textile Science and Engineering, Tiangong University, Tianjin 300387, China.

Supplementary Methods

Materials

N,N-Dimethylformamide (DMF, 99.5%); trtrahydrofuran (THF, 99.5%); dichloromethane (DCM, 99.5%); toluene (99.5%); 9,10-dibromoanthracene ($AnBr_2$, 98%); sodium methanolate (MeONa, 98%); trifluroacetic acid (TFA, 99%); triethylsilane (99%); poly(ethylene glycol) diacrylate (PEGDA, M_n~575) were purchased from Shanghai Titan Scientific *Co., Ltd.*

1,4-bis(4-(3-acryloyloxypropoxy)benzoyloxy)-2-methylbenzene (RM257, 98%); 3,6-dioxa-1,8-octanedithiol (EDDET, 99%); pentaerythritoltetrakis(3-mercapto-propionate) (PETMP, 95%); *S*-trityl-3-mercaptopropionic acid (TrtMPA, 98%), N-(3-Dimethylaminopropyl)-N'-ethylcarbodiimidehydrochloride (EDC, 99%), 4-(Dimethyl-amino)pyridine (DMAP, 98%) were provided by Bide Pharmatech *Co., Ltd.*

2-mercaptoethanol (99%), dipropylamine (DPA, 99%) were obtained from Shanghai Aladdin Biochemical Technology *Co., Ltd.* All chemicals were used as received.

Characterizations

^{1}H NMR. The chemical structures of the synthesized compounds were determined through ^{1}H nuclear magnetic resonance (AVANCE III HD 400, Bruker, Germany). The measurements were conducted at room temperature with chloroform-*d* ($CDCl_3$) and dimethyl sulfoxide-d_6 (DMSO-d_6) as the solvents, while tetramethyl silane (TMS) served as an internal standard. Results were shown in **Supplementary Fig. 1-3.**

Liquid Chromatography Mass Spectrometry (LC/MS). The molecular weight of final compound, $An(SH)_2$, was measured by Quadrupole Time of Flight LC/MS (Buker impact II, Bruker, Germany). Result was shown in **Supplementary Fig. 4**.

Attenuated Total Reflectance Fourier Transform Infrared Spectroscopy (ATR-

FTIR). A Fourier transform infrared spectrometer (iS20 Nicolet, ThermoFisher Scientific, America) is applied to monitor the procession of TAMAP. Mixed monomer solution before and after adding DPA was spin-coated on a silicon wafer. The spectra were recorded during thiol-acrylate Michael addition polymerization (TAMAP). The decrease of S-H bending (2570 cm^{-1}) and asymmetric C=C bending (1635 cm^{-1}) and C-H stretching (810 cm^{-1}) peaks revealed consumption of these groups, therefore indicated the TAMAP was in process, which were shown in **Supplementary Fig. 5**.

Swelling Test and Gel Fraction Measurement. Swelling test was used to confirm the formation of original crosslinked network of in AnLCE film. 3 pieces of AnLCE film with the size of 20 mm × 10 mm × 0.5 mm was soaked in 12 mL of DCM at a 15 mL glass vial. The vials were shaken by a roller shaft mixer for 24 h. The solvent in the vials, DCM, were replaced in the first 2, 4, 6 h. After swelling procession was completed, the swollen films were withdrawn from the vials and fully dried at 80 °C in a vacuum oven for 24 h to remove the solvent and got the final gel mass. The mass of AnLCE films before and after swelling test was denoted as M_0 and M_1, respectively. The swelling test data was shown in **Supplementary Table 2**. The final gelation fraction was calculated as 96.5% via Equation 1. As shown in **Supplementary Fig. 6**, the insoluble property and calculated high gelation fraction proved the formation of crosslinking network in AnLCE films.

$$Gel\ Fraction = \frac{M_1}{M_0} \times 100\% \quad (1)$$

Thermogravimetric Analysis (TGA). The thermogravimetric analysis was performed with a thermos gravimetric analyzer (TGA8000, PerkinElmer, America) at a heating rate of 10 °C min^{-1} and the temperature range was from room temperature to 500 °C with N_2 gas as carrier gas. The TG and DTG curves were shown in **Supplementary Fig. 7**, which indicated AnLCE is thermal stable with an onset temperature of decomposition (T_d) at about 300 °C

Mechanical Tensile Test: The cyclic uniaxial mechanical stretching was also conducted by DMA instrument (Discovery DMA 850, TA Instruments, America). By controlling the ambient temperature at 35 °C, the UV crosslinked AnLCE film and the untreated AnLCE film were stretched to 100% strain at a strain rate of 20%/min followed by a stress release to retract them. In addition, UV crosslinked AnLCE film with different maximum tensile strain (increased from 50% to 150%) was performed in the same ambient temperature and strain rate.

Laser Scanning Confocal Microscopy (LSCM). Surface morphology of AnLCE films were observed via LSCM (Olympus OLS5000 SAF, Olympus, Japan).

Polarized Optical Microscopy (POM). Polarized optical microscopic view was also acquired via LSCM by switching to the PO mode. As shown in **Supplementary Fig. 8**, the film showed a bright field at all directions which indicated the AnLCE film is in a polydomain state. When the film was uniaxially stretched to $2L_0$ and fixed, it showed a dark field in parallel and perpendicular to the polarizer (in the angle of 0° and 90°), while a bright field was observed at 45º. It revealed the film was oriented under stretching. When the stretching strain was removed, the film released back to original length, and it showed a bright field at all directions, which is same as its original POM observation before stretching. The phase transition upon heating was also monitored by POM. As shown in **Supplementary Fig. 11**, the birefringence of AnLCE film disappeared and turned into totally dark when the temperature was above 50 °C. It revealed the isotropic transition occurred. And the transition temperature range (50 – 60 °C) observed via POM was corresponding to the isotropic transition temperature determined by DMA. While the controlled elastomer, AnE, was observed in a same method.

X-Ray Diffraction (XRD). 2D-WAXS was performed via an WAXS/SAXS system (XEUSS, Xenocs, France) to determine the microstructure in AnLCE film. The 1D-

XRD spectrum was acquired by an X-Ray diffractometer (D8 Advance, Bruker, German). As shown in **Supplementary Fig. 9**,The diffusion ring at the wide-angle area in the 2D spectra of unstretched AnLCE film and a single diffraction peak found in 20° in 1D-XRD spectrum confirmed the non-oriented polydomain nematic phase.[1,2]

Dynamic Mechanical Analysis (DMA). Thermal transition of AnLCE upon heating was monitored by DMA (Discovery DMA 850, TA Instruments, America). An AnLCE film with the size of 30 × 5 × 0.5 mm^3 was heated from -50 °C to 100 °C at a heating rate of 5 °C min^{-1} in the tensile mode. The glass transition temperature (T_g = 21 °C) was measured at the turning point of storage modulus curve. And the isotropic transition temperature (T_{iso} = 55 °C) was determined by the end characteristic drop of storage modulus curve (**Supplementary Fig. 10**).

UV-Vis Spectroscopy. Absorbance spectra for thin film was measured by Ultraviolet-Visible Spectrophotometer (UV-2700i, Shimadzu, Japan). A thin AnLCE film attached on quartz slide was obtained by injecting monomer solution between 2 quartz slides via capillary force and subsequent TAMAP curing for 24 h. After 2 quartz slides were separated, the slide with AnLCE film was fully dried at a 70 °C oven for 24 h. The UV light intensity for irradiation on AnLCE thin film during UV test was controlled at 35 mW cm^{-2}. The UV light intensity was determined by a 365 nm UV illuminometer (UIT-101, Ushio, Japan). Resulted spectra were shown in **Supplementary Fig. 12**.

Atomic Force Microscopy (AFM). Surface modulus and depth-dependent cross section modulus variation was acquired by AFM (FastScan Bio, Bruker, Germany). While the ultrathin profile was obtained from an ultrathin sectioning system (LEICA EM UC7FC7, Leica, German). Result were shown in **Supplementary Fig. 13**.

Small Angle X-Ray Scattering (SAXS). The SAXS experiment was used to explored the orientation of the wrinkled films. Three AnLCE samples were selected for small-angle X-ray scattering (SAXS) experiment: **(1)** the raw AnLCE films, without any

treatment, was used to demonstrate the substrate; **(2)** the surface UV-exposed AnLCE films was exposed to UV light at an intensity of 35 mW/cm^2 for a period of 10 minutes. **(3)** the fully UV-crosslinked AnLCE film, which was exposed to a higher intensity (200 mW/cm^2) UV light for a period of 30 minutes on both sides, was used to demonstrate the UV-crosslinked top layer. The thickness of the sample films was controlled as approximately 130 μm. The SAXS experiments were then conducted on an Xeuss 2.0 WAXS/SAXS system (Xenocs, France). The wavelength of X-ray was 0.154 nm. And the X-ray detector was Pilatus 3R 300K, with single pixel size was 172 μm. During experiment, the distance between sample and detector was set to be 538.1 mm, and samples underwent X-ray exposure for 300 s. The scattering data of AnLCE films were acquired before stretching, under 200% stretching ($3L_0$) and after releasing to their original length, respectively.

The SAXS results of (1) raw AnLCE, (2) surface crosslinked AnLCE and (3) fully crosslinked AnLCE film were shown in **Supplementary Fig. 26**. The 3 AnLCE films did not displayed apparently anisotropic character before stretching. After releasing from 200% stretching, evident orientation was found in the scattering images of surface crosslinking and fully crosslinking AnLCE film, and none obvious orientation was found in the raw AnLCE sample due to the recovery of the polydomain phase. These results indicated the liquid crystal orientation in the UV-crosslinked top layer after stretching-releasing.

Synthesis of 9,10-bis((2-(hydroxy) ethyl) thio) anthracene ($An(OH)_2$)

The synthesis in this step is as description of literature.[3] 40 mmol of $AnBr_2$ was added into a flask, and then, 120 mL of DMF was added in. After 100 mmol of MeONa and 100 mmol of 2-mercaptoethanol was added in, the flask was protected by nitrogen gas. The system was subsequently heated to 100 °C and stirred for 6 h. As the reaction runs, the mixture changes from yellow suspension into dark-red solution. After the reaction was completed, the reaction mixture was poured into 600 mL of deionized water, the yellow precipitate was collected and was by 500 mL water again. The precipitate was washed by 200 mL of DCM for 30 min for further purification. The resulting purified product was dried at a 50 °C vacuum oven for 12 h.

The resulting product, $An(OH)_2$, was obtained as yellow powder in 90% yield. The structure of $An(OH)_2$ was confirmed by its ^1H NMR spectrum, as shown in **Supplementary Fig. 1.**

An(OH)$_2$ ^1H NMR (500 MHz, DMSO-d6) δ 9.06 – 8.97 (m, 4H, 1,4,5,8-Anthracene **H**), 7.77 – 7.70 (m, 4H, 2,3,6,7-Anthracene **H**), 4.82 (t, J = 5.5 Hz, 2H, -O**H**), 3.39 (td, J = 6.8, 5.4 Hz, 4H, -C**H**$_2$-OH), 2.97 (t, J = 6.8 Hz, 4H, -C**H**$_2$-S-An).

Synthesis of 9,10-bis((2-((3-(tritylthio) propanoyl) oxy) ethyl) thio) anthracene ($An(Trt)_2$)

16 mmol of $An(OH)_2$, 40 mmol of TrtMPA, 64 mmol of EDC, and 1.6 mmol of DMAP was added into a 500 mL flask. After 250 mL THF was adding in, the mixture was stirred at room temperature for 24 h. As the reaction runs, the solid reactant, $An(OH)_2$ was gradually dissolved and form a clear solution. After the reaction was completed, the product was precipitated by pouring the reaction mixture into 600 mL of EtOH. The solid was collected and wash by hot EtOH (50 °C) again. The product was dried in vacuum at 50 °C for 12 h.

The resulting product, $An(Trt)_2$, was obtained as yellowish powder in 85% yield.

Its chemical structure was verified by ^{1}H NMR, which is shown in **Supplementary Fig. 2.**

An(Trt)$_2$ ^{1}H NMR (400 MHz, Chloroform-*d*) δ 9.04 – 8.92 (m, 4H, 1,4,5,8-Anthracene **H**), 7.62 – 7.53 (m, 4H, 2,3,6,7-Anthracene **H**), 7.45 – 7.15 (m, 30H, benzene **H**), 3.98 (t, *J* = 6.5 Hz, 4H, -C**H**$_2$-O-), 3.06 (t, *J* = 6.5 Hz, 4H, -C**H**$_2$-S-An), 2.34 (t, *J* = 7.4 Hz, 4H, -C**H**$_2$-S-Trt), 2.04 (t, *J* = 7.4 Hz, 4H, -C**H**$_2$-CO-O-).

Synthesis of dithiol monomer, 9,10-bis((2-(3-mercaptopropanoyl) oxy) ethyl) thio) anthracene (An(SH)$_2$)

The deprotection of trtyl groups was performed as literature description.[4] 5 mmol An(Trt)$_2$ and 15 mmol of triethylsilane (Et_3SiH) were in 100 mL of DCM. 10 mL of TFA was then added into the solution and stirred for 1 h. After the reaction was completed, the mixture was washed by deionized water for 3 times to remove TFA, while the organic phase was collected and dried by anhydrous sodium sulfate. was sufficiently mixed with 2 times volume of *n*-hexane.

The mixture was heated to 50 °C and remove part of the solvent by rotary evaporator. When the solution turned to slightly turbid, heating and evaporation was stopped, the solution was cooled down to room temperature. During cooling, crystallization occurred and generated yellow crystal. Crystallization could be accelerated by further cooling to -20 °C. The solid was collected and washed by 50 °C *n*-hexane. The resulting product underwent 50 °C vacuum for 12 h.

The final product was obtained as yellow needle-like crystal in 85% yield. Its structure was confirmed by ^{1}H NMR, which is shown in **Supplementary Fig. 3**. Furthermore, its molecular weight was verified by LC/MS, which is shown in **Supplementary Fig. 4**.

An(SH)$_2$ ^{1}H NMR (400 MHz, DMSO-d_6) δ 9.04 – 8.95 (m, 4H, 1,4,5,8-Anthracene **H**), 7.80 – 7.71 (m, 4H, 2,3,6,7-Anthracene **H**), 4.01 (t, *J* = 6.0 Hz, 4H -C**H**$_2$-O-), 3.19 (d,

J = 12.1 Hz, 4H, -C**H**$_2$-S-An), 2.45 (qd, *J* = 7.4, 1.4 Hz, 4H, -C**H**$_2$-SH), 2.35 (dd, *J* = 8.9, 7.2 Hz, 2H, -CH$_2$-S**H**), 2.26 (t, *J* = 7.0 Hz, 4H, -C**H**$_2$-CO-O-).

Preparation of fully UV-crosslinked AnLCE thin film

The UV treated film with fully crosslinking via anthracene's dimerization was fabricated by utilizing a thin molding box with approximately 200 μm spacer. After TAMAP, the box was opened and the film was dried at 80 °C at a vacuum oven for 24 h. The thickness of AnLCE samples were approximately 130 μm after solvent evaporation.

Both side of the thin films were irradiated for 60 min to ensure the full crosslinking. The crosslinking of the thin film was verified by the absence of fluorescence under 365 nm UV light.

A simple tensile test was performed by stretching a crosslinked film to 100% strain, after releasing, the film did not recover its length with about 30% residual strain. The film was heated to 100 °C to recovered its length, which is shown in **Supplementary Fig. 19**.

Stability test for wrinkled AnLCE films

An AnLCE film was irradiated by UV for 600 s at the intensity of 35 mW cm^{-2}, subsequently SR cycles was applied for fabricating uniform surface wrinkle perpendicular to the SR direction. The sample was store at 29 °C in a thermostat, and the characteristic sizes of surface wrinkles, including wavelength and amplitude were recorded by LSCM within the first 3 days and the last 2 days. Results were shown in **Supplementary Fig. 16**.

Preparation of controlled elastomer film

The controlled elastomer films, AnE, without LC gen were synthesis by TAMAP in the similar process to our AnLCE. In this system, the LC monomer, RM 257, was replaced by amorphous monomer, PEGDA, with number average molecular weight, M_n = 575. The mole ratio of PEGDA/ $An(SH)_2$/EDDET/PETMP/Irgacure 784 is 115/40/40/10/2. The monomer mixture containing 1.15 mmol of PEGDA, 0.4 mmol of $An(SH)_2$, 0.4 mmol of EDDET and 0.1 mmol of PETMP and 0.02 mmol of initiator, I 784, were dissolved in 0.4 g of toluene at 80 °C. When the mixture was totally melted to a clear liquid, 100 mg of DPA/toluene solution was added to the mixture to catalyze the TAMAP reaction. After overnight TAMAP reaction, the mixture was irradiated by green light for fully cure via radical photo polymerization initiated by I 784. The AnE films were finally dried at 80 °C in a vacuum oven for 12 h.

The fabricated AnE was much weaker than AnLCE. Its breaking elongation was typically less than 100%.

Fabricating wrinkle pattern on AnE film by UV-SR

The strategy "UV-SR" was first tried to fabricate wrinkle pattern on AnE film. The AnE film was irradiated by UV at the intensity of 35 mW cm^{-1} for 800 s. The film was subsequently stretched to $1.5L_0$ and released. During releasing, no wrinkle formed on the AnE surface, detailed result was showed in **Supplementary Fig. 23**.

Fabrication of surface wrinkle on AnE film by S-UV-R its thermal manipulation

Conventional strategy "S-UV-R" (stretching-UV exposure-releasing) was used for fabricating wrinkle patterns on AnE's surface. As shown in **Supplementary Fig. 24a**. the AnE film was stretched to $1.5L_0$ and subsequently exposed to UV at the intensity

of 35 mW cm^{-1} for 800 s, wrinkle formed on the surface of AnE after releasing.

The AnE film with wrinkle pattern on the surface (fabricated via S-UV-R) was placed on a 100 °C heat plate and kept for 1 h. wrinkle dimension was measured each 15 min. Wrinkle on AnE surface was not erased during and after heating, which is shown in **Supplementary Fig. 24b.**

Fabrication of surface wrinkle on AnLCE film by S-UV-R and its thermal manipulation

Conventional strategy "S-UV-R" for fabricating wrinkle patterns on AnLCE's surface was used. **Supplementary Fig. 25a** illustrated the process. The AnLCE film was stretched to $2L_0$ and irradiated by UV light at the intensity of 35 mW cm^{-1} for 600 s. After releasing the stress, wrinkle formed on AnLCE' surface.

Supplementary Fig. 25b showed the thermal response of AnLCE's surface wrinkle fabricated by S-UV-R. When the film was heated to 100 °C, the surface wrinkle was erased. After cooling down, the wrinkle did not recover.

Supplementary Discussion

The wrinkle evolution with increasing stretching ratio

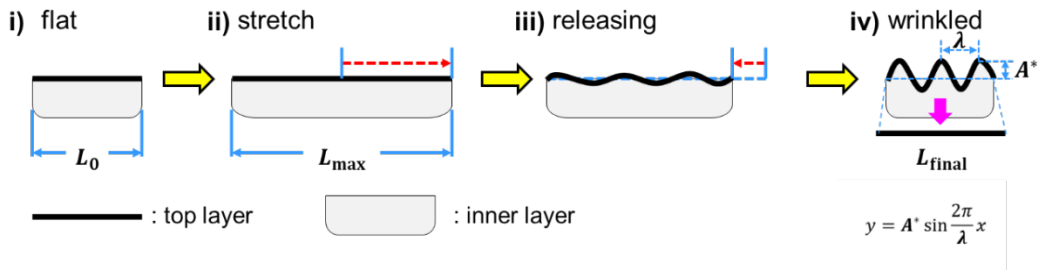

Supplementary Note 1. The illustration of evolution on top layer during stretching and releasing along the profile of SR direction

The wrinkle evolution with increasing stretching ratio was studied. The evolution of top layer during stretching-releasing was illustrated in **Supplementary Note 1**. We described the wrinkle profile along the SR direction (x) as a sinusoid wave:

$$y = \boldsymbol{A}^* \sin\frac{2\pi}{\boldsymbol{\lambda}}x \tag{3}$$

Where $A^* = 0.5A$ and λ represented the amplitude and is the wavelength in this sinusoid function, respectively. The residual strain was therefore calculated by following Supplementary Equation (4). The residual strain for different stretching ratio was shown in **Supplementary Table 2**.

$$Residual\ \ Strain = \frac{L_{\text{final}} - L_0}{L_0} = \frac{\int_0^{\lambda} \mathrm{d}L}{\lambda} - 1 = \frac{\int_0^{\lambda} \sqrt{1 + (y')^2}\,\mathrm{d}x}{\lambda} - 1$$
$$= \frac{\int_0^{\lambda} \sqrt{1 + \left(\frac{2\pi A^*}{\lambda}\cos x\right)^2}\,\mathrm{d}x}{\lambda} - 1 \tag{4}$$

According to the calculation, the residual strain of top layer increased with the

stretching ratio and reached the maximum at 100% stretching strain. But further increasing in stretching ratio would not increase the residual strain. Meanwhile, the $L_{\mathrm{final}} < L_{\mathrm{max}}$ indicated the partial recovery of top layer during releasing.

The evolution of wrinkle with increasing UV irradiation time

The characteristic sizes of wrinkle system, wavelength (λ) and amplitude (A), are quantitatively described by these following equations:

$$\lambda = 2\pi h_{\mathrm{f}} \left(\frac{E_{\mathrm{eff}}}{3\overline{E_{\mathrm{s}}}} \right)^{1/3}, E_{\mathrm{eff}} = \overline{E_{\mathrm{f}}} + \frac{\overline{E_{\mathrm{s}}} - \overline{E_{\mathrm{f}}}}{4\left(h_{\mathrm{f}}/h_{\mathrm{g}} + 1\right)^3} \tag{5}$$

$$A = (h_{\mathrm{f}} + h_{\mathrm{g}}) \left(\frac{\varepsilon_0}{\varepsilon_c} - 1 \right)^{1/3}, \varepsilon_c = -\frac{1}{4} \left(\frac{3\overline{E_{\mathrm{s}}}}{E_{\mathrm{eff}}} \right)^{2/3} \tag{6}$$

Where the subscript f, g and s represent the top layer toward UV irradiation, gradient crosslinking layer and substrate backward UV irradiation, respectively. While h_{f} and h_{g} represents the thickness of top layer and gradient layer. $\overline{E_{\mathrm{f}}} = E_{\mathrm{f}}/(1-\nu_f^2)$ and $\overline{E_{\mathrm{s}}} = E_{\mathrm{s}}/(1-\nu_s^2)$ are plane strain modulus of the top layer and substrate. The ε_0 and ε_c represent compressive strain and critical threshold strain, respectively.

When the stretching strain was kept constantly 100% and generated 37% residual strain. The compressive strain, ε_0, in Supplementary Equation 5 was kept constant. Meanwhile, the increase of UV exposure time increased the thickness of crosslinking layer (h_{f} and h_{g} values in Supplementary Equation 5 and 6). It finally led to the increase in both the wavelength and amplitude.

Supplementary Tables

Supplementary Table 1. Swelling test of AnLCE in DCM

Sample	M_0(g)	M_1(g)	Gel fraction (%)
1#	0.121	0.117	96.69
2#	0.117	0.113	96.58
3#	0.106	0.102	96.23

Supplementary Table 2. The wrinkle evolution with increasing stretching ratio

Stretching ratio	L_{max}	A^*	λ	A/λ	Residual Strain
50%	1.50 L_0	0.15	1.24	0.237	0.13
75%	1.75 L_0	0.18	1.14	0.318	0.21
100%	2.00 L_0	0.21	0.97	0.429	0.37
125%	2.25 L_0	0.18	0.83	0.449	0.37
150%	2.50 L_0	0.17	0.77	0.440	0.37

Supplementary Figures

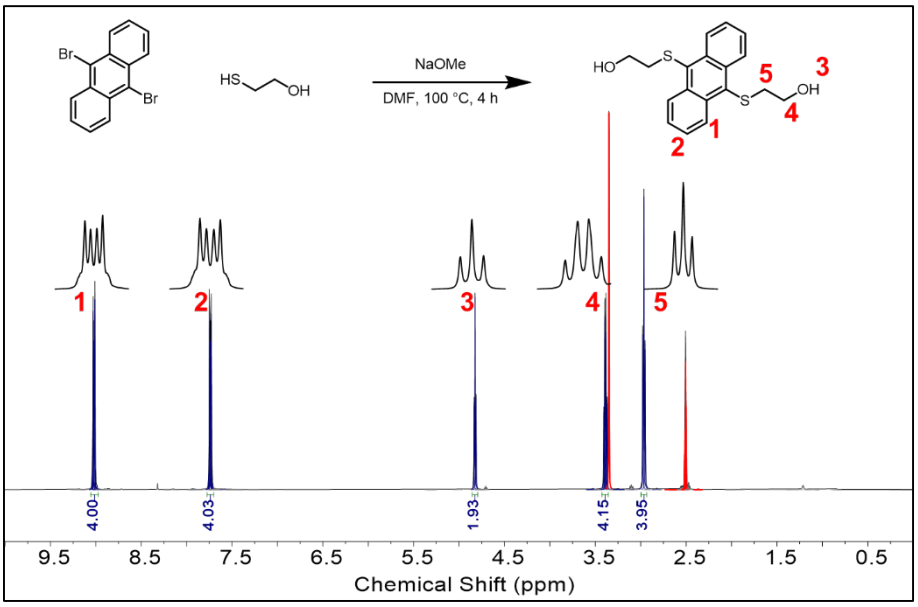

Supplementary Fig. 1. Synthesis route of An(OH)$_2$ and its ^{1}H NMR spectrum in DMSO-*d*$_6$ solution at 298 k.

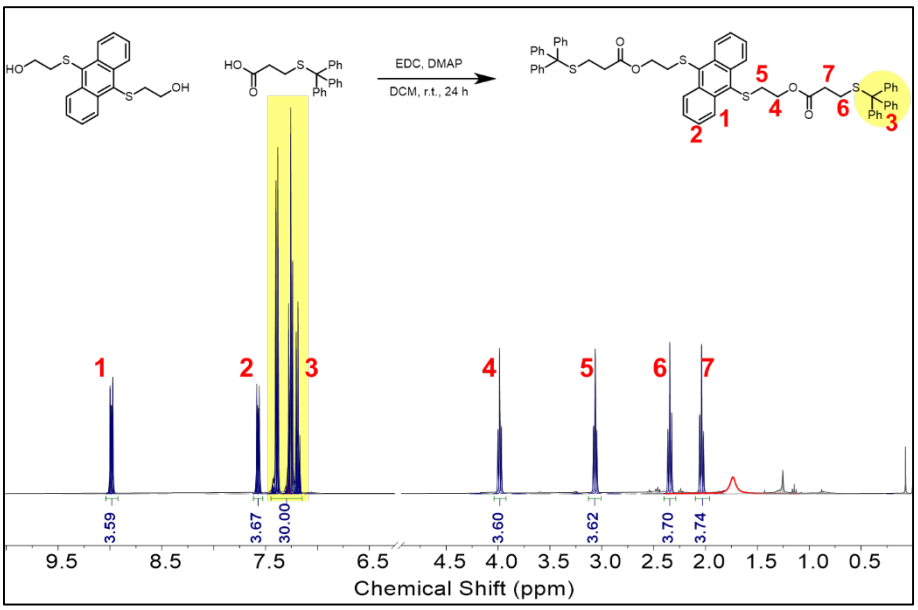

Supplementary Fig. 2. Synthesis route of An(Trt)$_2$ and its ^{1}H NMR spectrum in chloroform-*d* solution at 298 k.

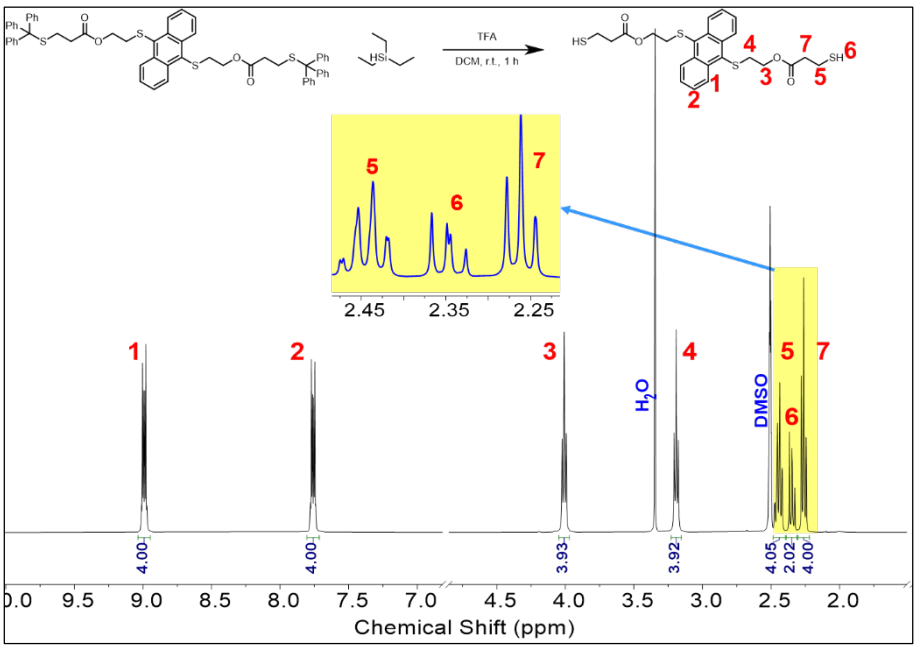

Supplementary Fig. 3. Synthesis route of $An(SH)_2$ and its ^1H NMR spectrum in DMSO-d_6 solution at 298 k.

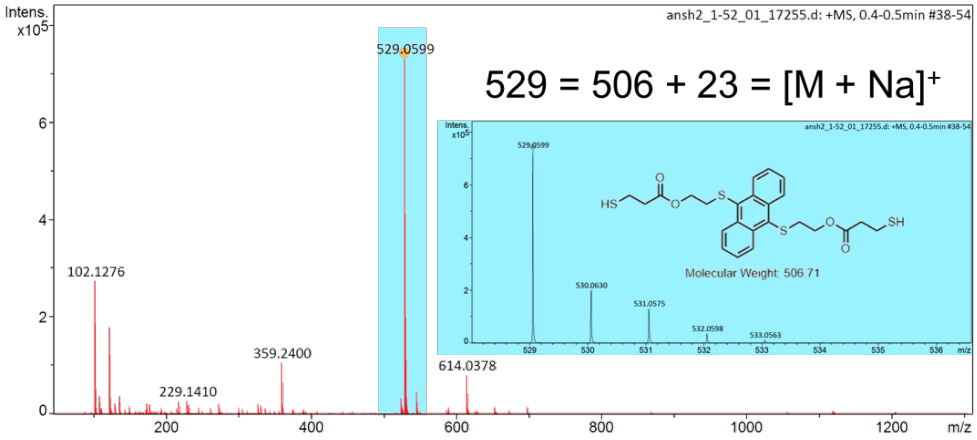

Supplementary Fig. 4. MS spectra for $An(SH)_2$ at 298 k.

LCMS (ESI) ($[M+Na]^+$, $C_{24}H_{26}O_4S_4Na$): calculated, 529.70; found, 529.0599.

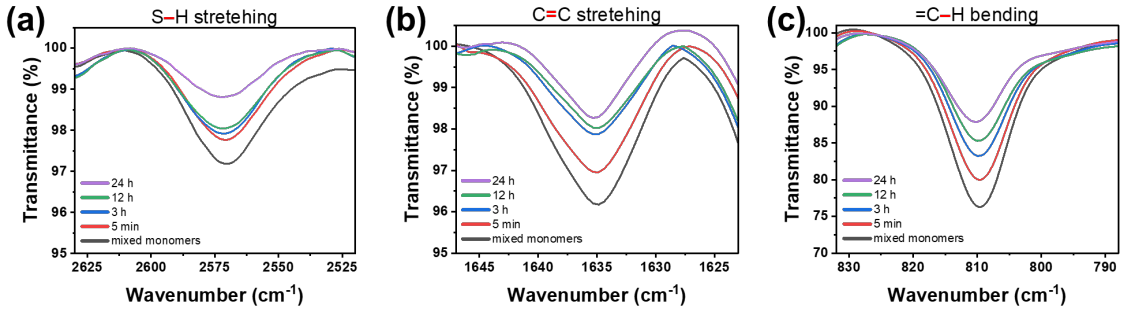

Supplementary Fig. 5. IR spectra of monomer mixture during TAMAP.

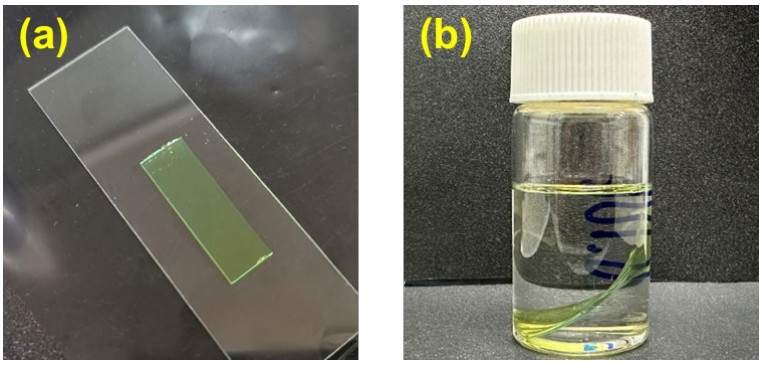

Supplementary Fig. 6. AnLCE film (a) before and (b) after swelling in DCM.

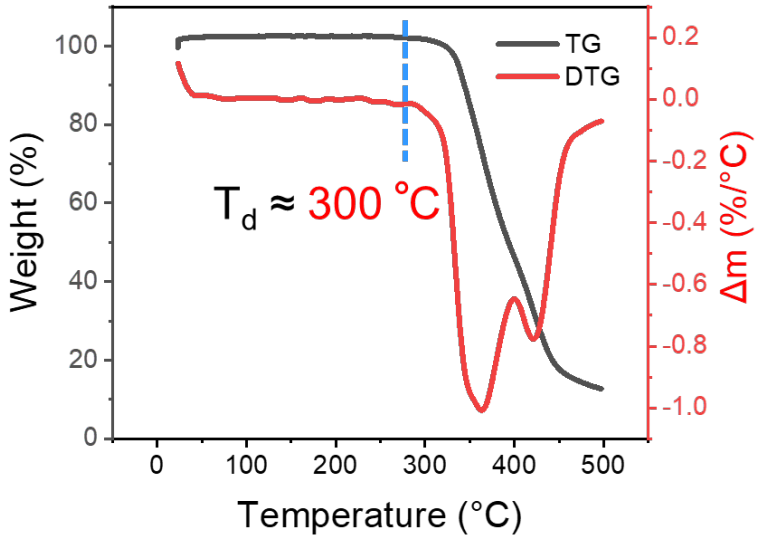

Supplementary Fig. 7. TG and DTG curves of AnLCE film

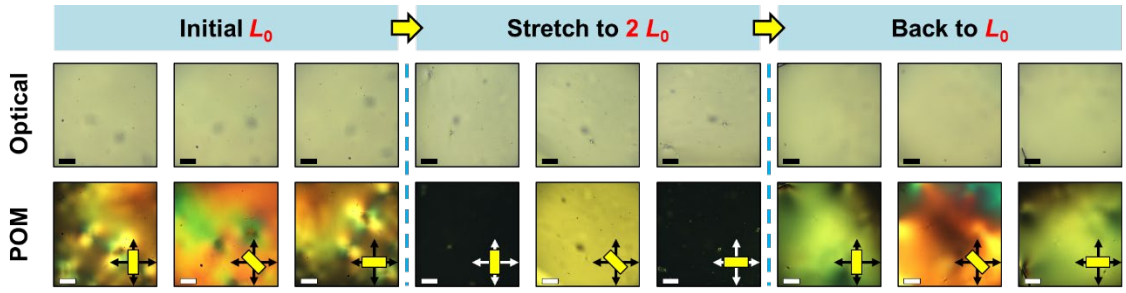

Supplementary Fig. 8. Optical and polarized optical images of AnLCE film before and under uniaxial stretching and after releasing back to original length. Scale bar: 200 μm.

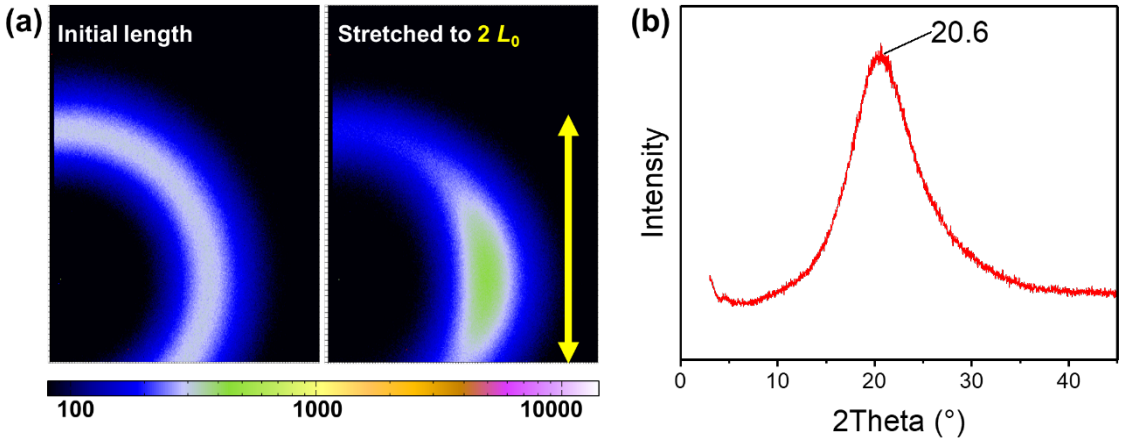

Supplementary Fig. 9. Wide-angle X-ray scattering spectra of AnLCE film. (a) 2D WAXS pattern of AnLCE film before and after stretching. **(b)** 1D XRD spectrum of AnLCE film without stretching.

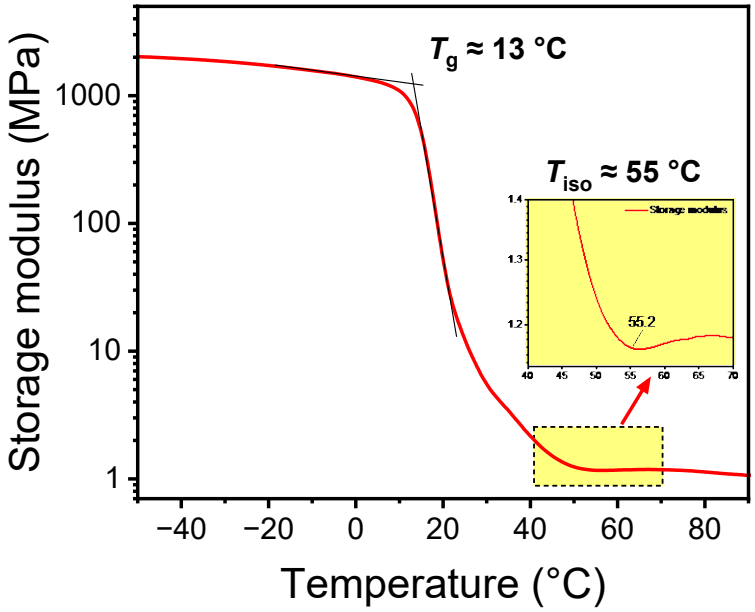

Supplementary Fig. 10. DMA curves of AnLCE.

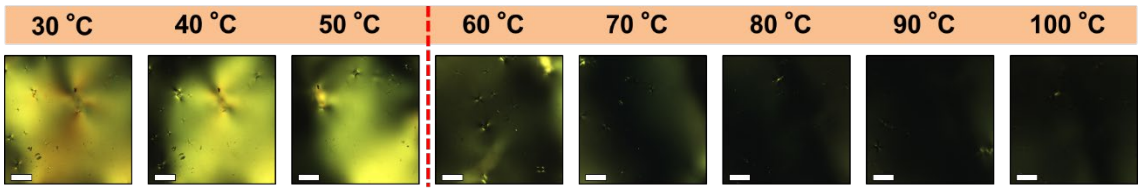

Supplementary Fig. 11. POM images of AnLCE film upon heating. Scale bar: 200 μm.

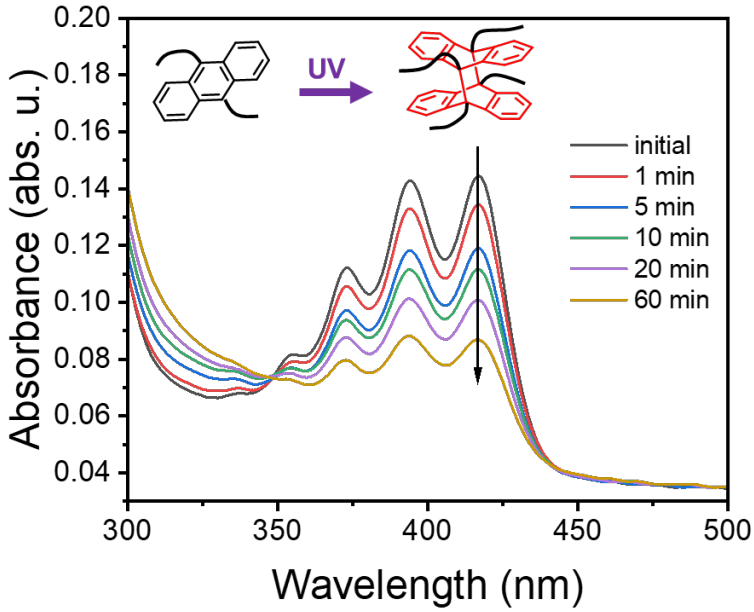

Supplementary Fig. 12. UV-Vis spectra of AnLCE film during the photo-dimerization upon

365 nm UV irradiation at the intensity of 35 mW cm^{-2}.

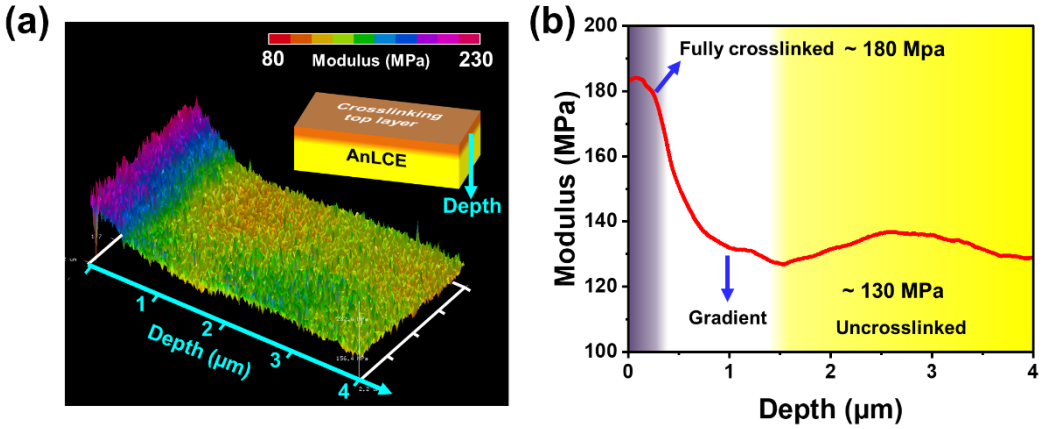

Supplementary Fig. 13. Cross-sectional modulus of UV treated AnLCE film acquired by AFM. Modulus map **(a)** and profile **(b)** along depth direction. The AnLCE film was treated by UV irradiation for 600 s at the intensity of 35 mW cm^{-2}.

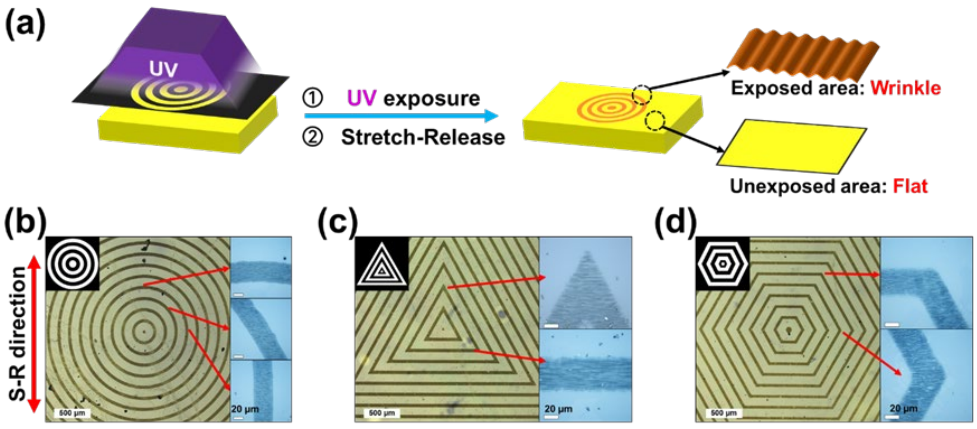

Supplementary Fig. 14. Hierarchical pattern fabricated by utilizing photomasks. (a) Schematic illustration patterned wrinkle surface fabricated by utilizing photomasks. **(b-d)** Different hierarchical pattern fabricating via photomasks, including **(b)** concentric circle, **(c)** triangle, **(d)** hexagon.

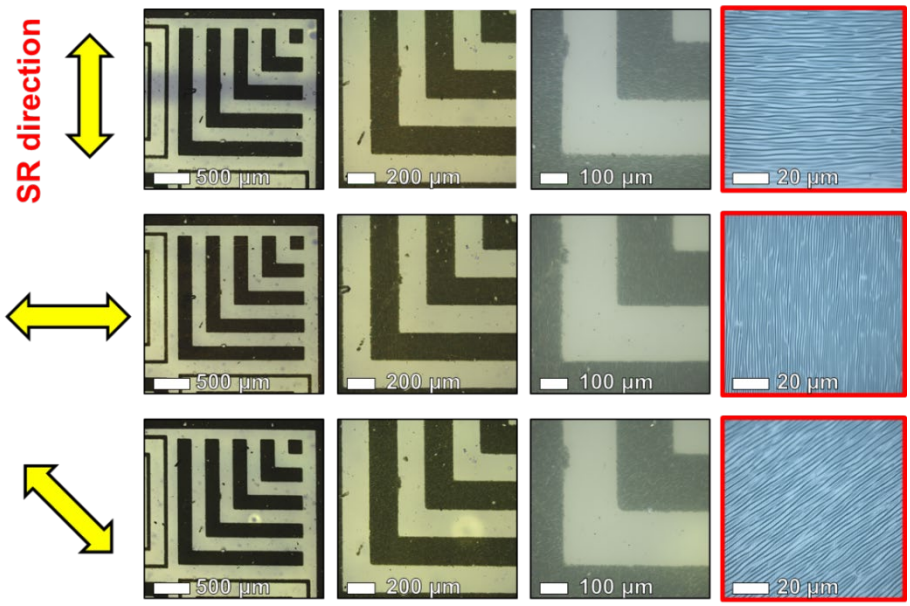

Supplementary Fig. 15. Different orientation of micro wrinkle in the same macroscopic pattern obtained by changing stretching-releasing directions.

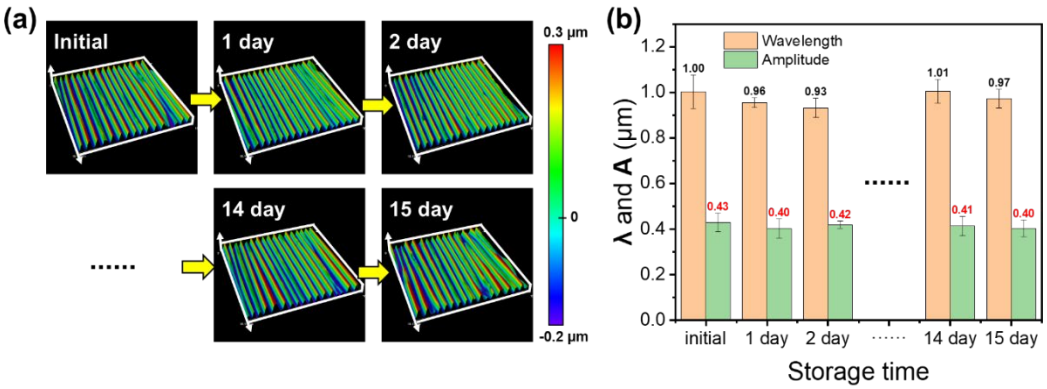

Supplementary Fig. 16. 15-day stability test of surface wrinkle on AnLCE film. (a) Morphologies of surface wrinkle during 15-day storage. **(b)** The statistical data of characteristic wavelength and amplitude during 15-day storage. Results are shown as mean ± SD, n = 6.

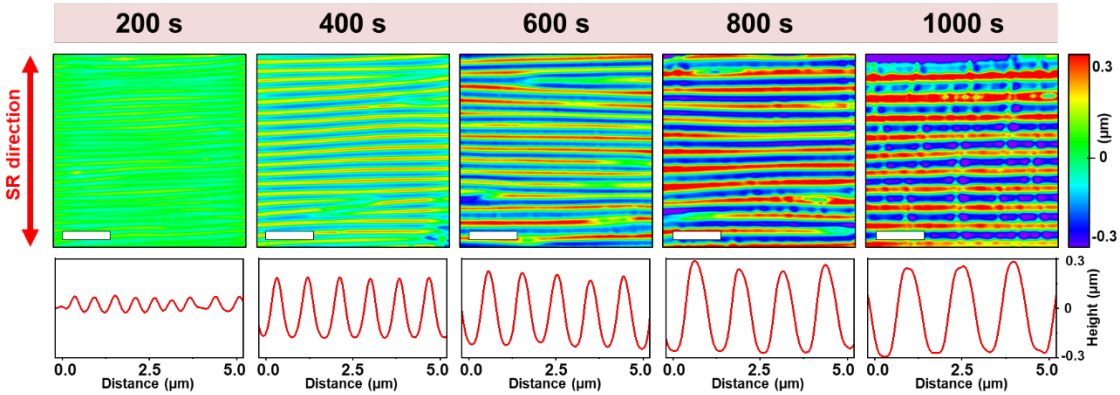

Supplementary Fig. 17. The evolution of surface wrinkle and their corresponding profile to increasing UV exposure time.

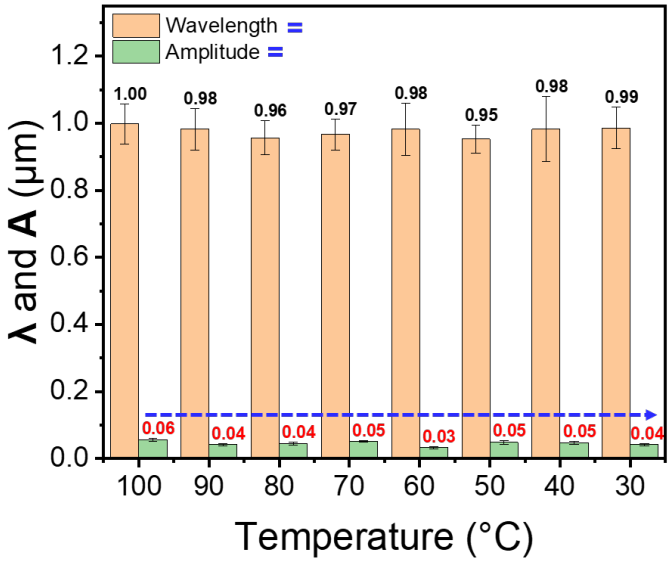

Supplementary Fig. 18. The evolution of AnLCE surface wrinkle upon cooling from 100 °C to 30 °C Results are shown as mean ± SD, n = 6.

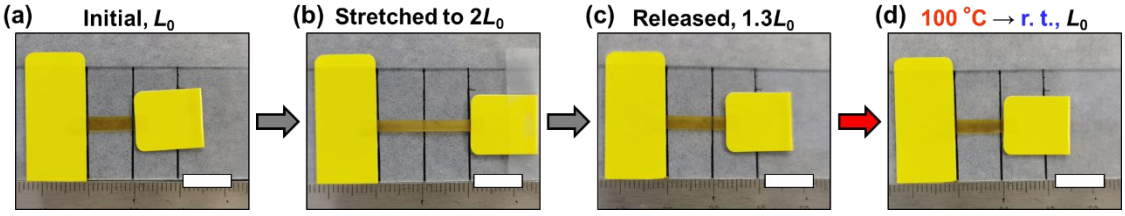

Supplementary Fig. 19. Thermal deformation of crosslinked AnLCE film upon heating to illustrated the erasure of wrinkled layer. **(a)** A crosslinked AnLCE film in its initial length, **(b)** film under stretching to 100% strain, **(c)** after releasing, **(d)** after heating to 100 °C and cooled down to room temperature. Scale bar: 1 cm.

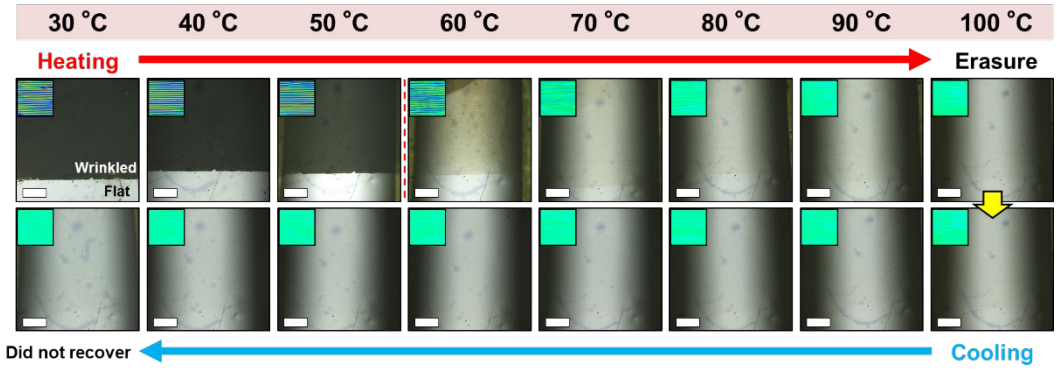

Supplementary Fig. 20. The thermal stimuli transition of wrinkle film via optical view in low magnification (5×). The initially black area is wrinkled area, while the blank area is flat. The insets are laser scanning view at the wrinkle area (16 μm × 16 μm) corresponding to Fig. 3a. Scale bar: 500 μm.

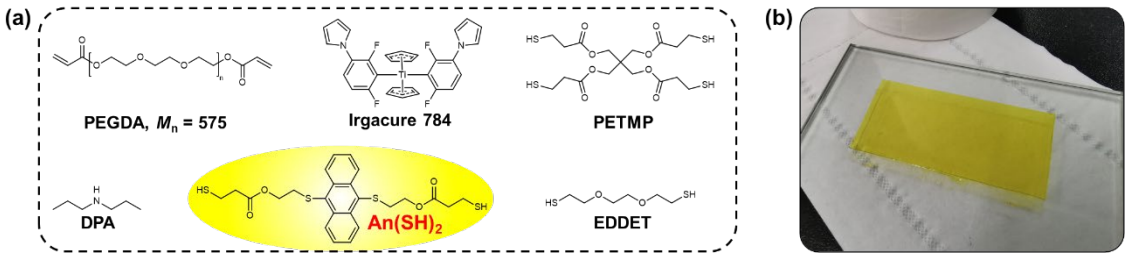

Supplementary Fig. 21. Synthesis of controlled elastomer, AnE. (a) Chemicals for fabricating controlled AnE. **(b)** A photograph of prepared AnE film.

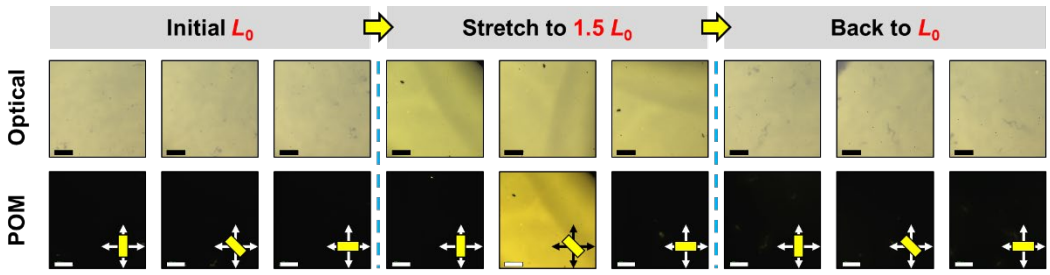

Supplementary Fig. 22. Optical and polarized optical microscopic images of controlled AnE film before and after uniaxial stretching. Scale bar: 500 μm.

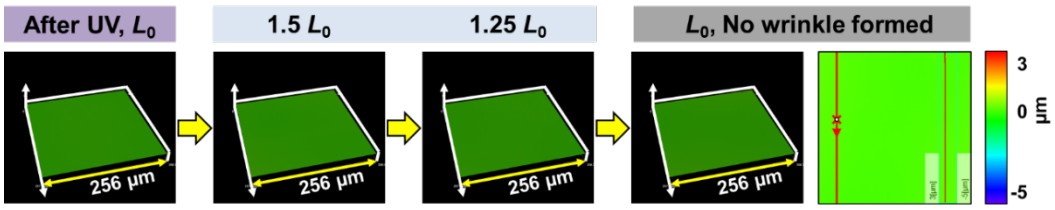

Supplementary Fig. 23. Attempt to fabricate surface wrinkle by UV-SR on the surface of controlled AnE.

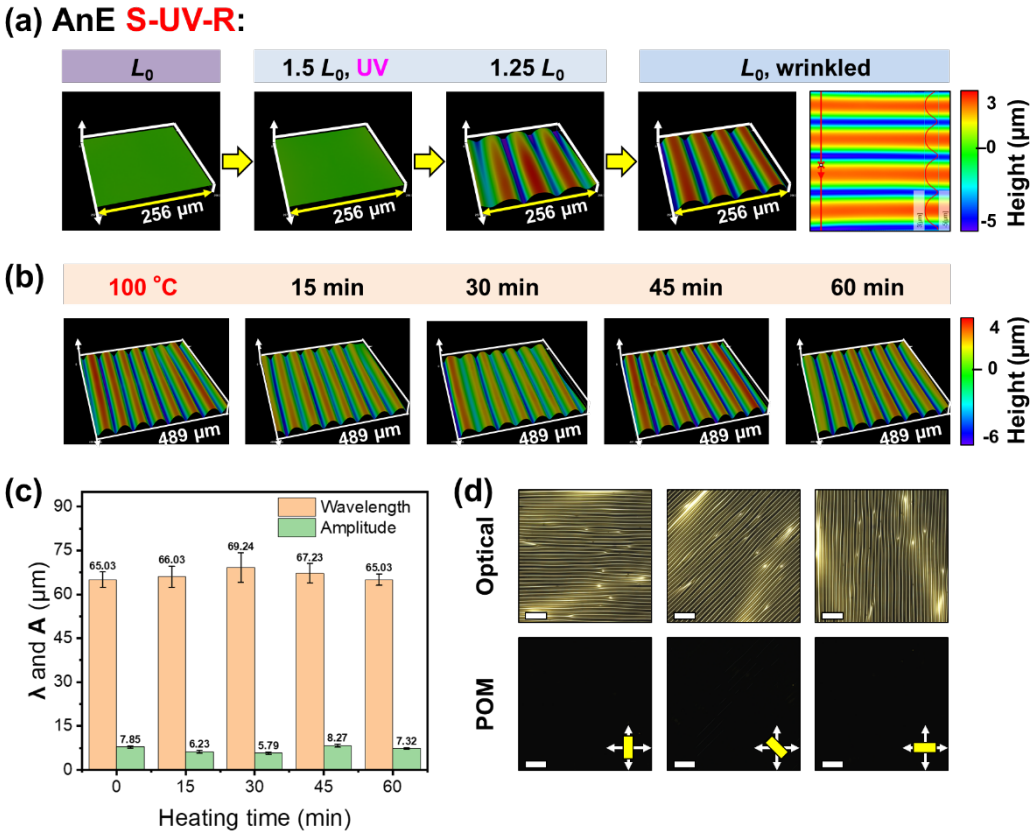

Supplementary Fig. 24. Thermal and optical properties of surface wrinkle on AnE generated by S-UV-R. (a) Fabrication surface wrinkle by UV-SR on controlled elastomer AnE. **(b)** and **(c)** The surface morphology monitoring and corresponding data upon 100 °C heating for 60 min. Results are shown as mean ± SD, n = 6. **(d)** Optical and polarized optical images of wrinkled AnE surface. Scale bar: 200 μm.

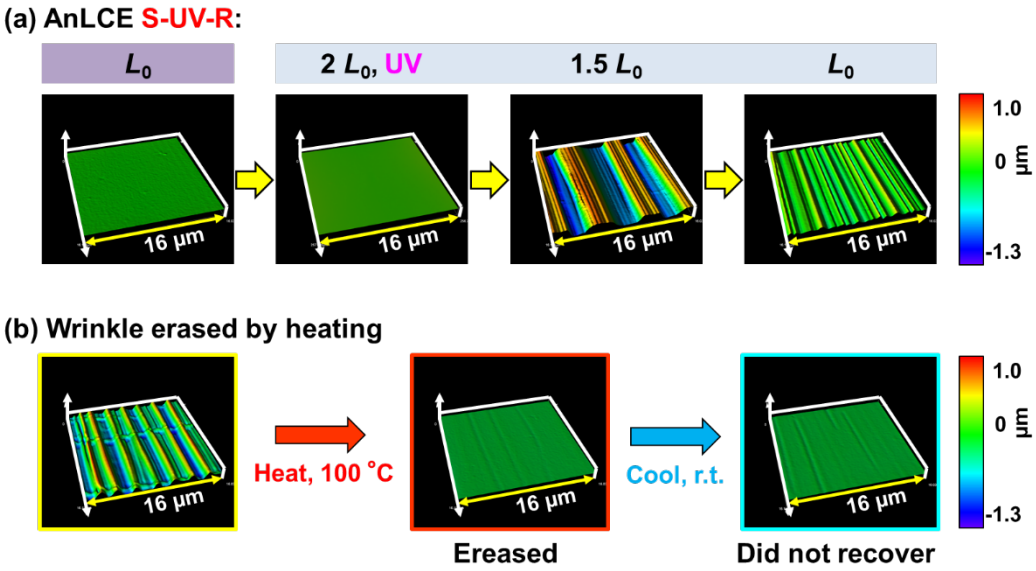

Supplementary Fig. 25. Fabrication of surface wrinkle on AnLCE film by S-UV-R (a) and its thermal response (b).

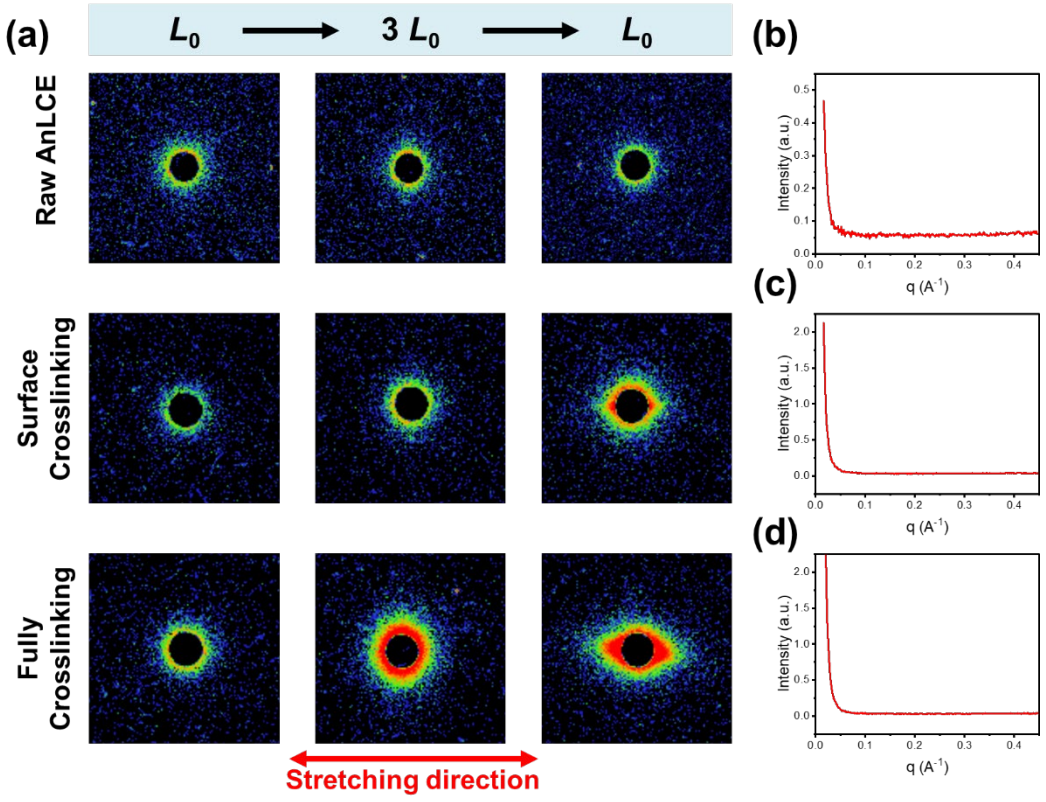

Supplementary Fig. 26. The SAXS results of different AnLCE films (a) The scattering images of AnLCE films before stretching, under 200% stretching and after releasing, respectively. **(b-d)** The q spectra derived from the scattering images after releasing. Spectra designated **(b), (c), (d)**

corresponded to the raw AnLCE, surface crosslinked AnLCE and fully crosslinked AnLCE film, respectively.

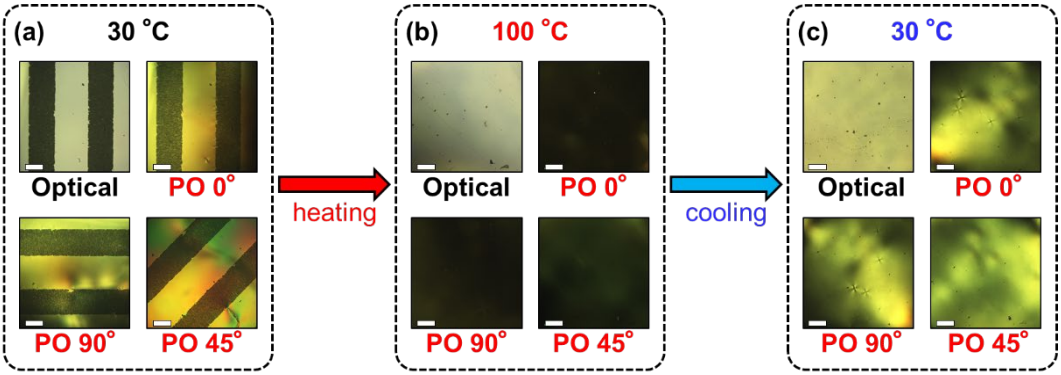

Supplementary Fig. 27. Optical and polarized optical microscopy images of patterned AnLCE film (a) at 30 °C, (b) at 100 °C and (c) after cooling down to 30 °C. Scale bar: 200 μm.

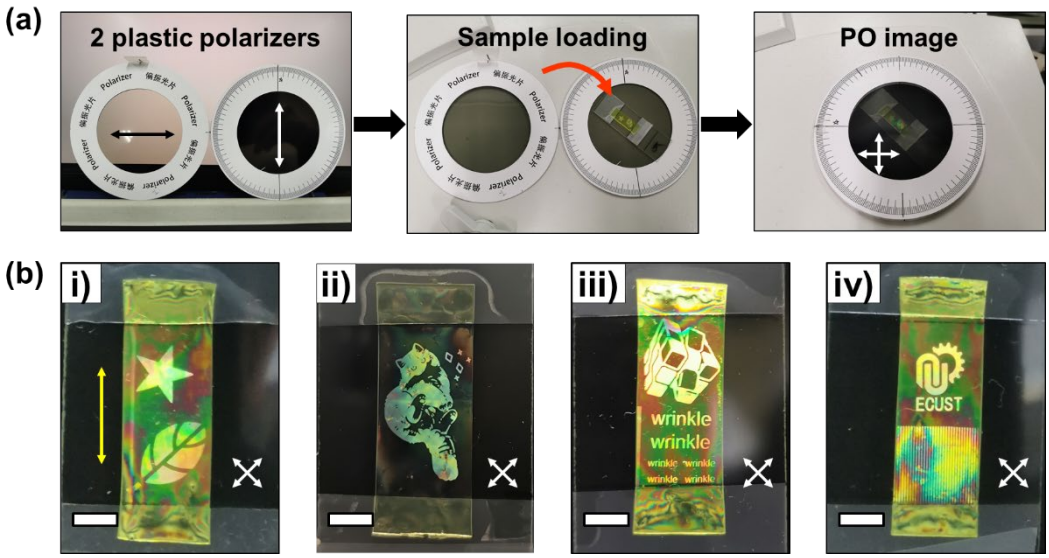

Supplementary Fig. 28. Polarized optical images observed by utilizing plastic crossed polarizers. (a) Process of observing AnLCE surface pattern via plastic crossed polarizers. (b) PO images with various patterns on AnLCE's surface. The white cross arrows in indicated the orientation of the 2 crossed polarizers, while the yellow arrow was the SR direction of AnLCE films. Scale bar: 0.5 cm.

Supplementary References

1 Ohzono, T., Minamikawa, H., Koyama, E. & Norikane, Y. Unlocking Entropic Elasticity of Nematic Elastomers Through Light and Dynamic Adhesion. *Adv. Mater. Interfaces* **8**, 2100672, doi:10.1002/admi.202100672 (2021).

2 Fan, Y. *et al.* One-Step Manufacturing of Supramolecular Liquid-Crystal Elastomers by Stress-Induced Alignment and Hydrogen Bond Exchange. *Angew. Chem. Int. Ed.* **62**, 202308793, doi:10.1002/anie.202308793 (2023).

3 Lei, J. *et al.* 9,10-Dithio/oxo-Anthracene as a Novel Photosensitizer for Photoinitiator Systems in Photoresists. *Macromol. Chem. Phys.* **220**, 1900152, doi:10.1002/macp.201900152 (2019).

4 Harnoy, A. J., Papo, N., Slor, G. & Amir, R. J. Mixing End Groups in Thiol-Ene/Yne Reactions as a Simple Approach toward Multienzyme-Responsive Polymeric Amphiphiles. *Synlett* **29**, 2582-2587, doi:10.1055/s-0037-1611340 (2018).